

# Interpretable (not just posthoc-explainable) medical claims modeling for discharge placement to reduce preventable all-cause readmissions or death

Joshua C. Chang,<sup>1</sup> Ted L. Chang,<sup>1</sup> Carson C. Chow,<sup>2</sup> Rohit Mahajan,<sup>1</sup> Sonya Mahajan,<sup>1</sup>  
Shashaank Vattikuti,<sup>1</sup> Hongjing Xia,<sup>1</sup>

<sup>1</sup>Mederrata, United States of America

<sup>2</sup>NIH NIDDK, United States of America

## Abstract

This manuscript addresses the simultaneous problems of predicting all-cause inpatient readmission or death after discharge, and quantifying the impact of discharge placement in preventing these adverse events. To this end, we developed an inherently interpretable multilevel Bayesian modeling framework inspired by the piecewise linearity of ReLU-activated deep neural networks. In a survival model, we explicitly adjust for confounding in quantifying local average treatment effects for discharge placement interventions. We trained the model on a 5% sample of Medicare beneficiaries from 2008 and 2011, and then tested the model on 2012 claims. Evaluated on classification accuracy for 30-day all-cause unplanned readmissions (defined using official CMS methodology) or death, the model performed similarly against XGBoost, logistic regression (after feature engineering), and a Bayesian deep neural network trained on the same data. Tested on the 30-day classification task of predicting readmissions or death using left-out future data, the model achieved an AUROC of approximately 0.76 and and AUPRC of approximately 0.50 (relative to an overall positive rate in the testing data of 18%), demonstrating how one need not sacrifice interpretability for accuracy. Additionally, the model had a testing AUROC of 0.78 on the classification of 90-day all-cause unplanned readmission or death. We easily peer into our inherently interpretable model, summarizing its main findings. Additionally, we demonstrate how the black-box posthoc explainer tool SHAP generates explanations that are not supported by the fitted model – and if taken at face value does not offer enough context to make a model actionable.

## Introduction

The overarching goal of any healthcare system is to enhance the health of the patients it serves. Resources, including healthcare dollars, are a primary limitation to achieving this goal. A secondary limitation is preventable harm inadvertently caused by the delivery of healthcare. Preventable harm also unfortunately contributes to overall healthcare dollars consumed as redundant care is administered to compensate for the harm inflicted. Readmission to the hospital as well as adverse events related to medical care have been identified as two kinds of incidents that are associated with increased

healthcare spending and preventable harm. For example, in 2011 it was estimated that the hospital costs for adult 30-day all cause hospital readmission in the United States was about \$41.3 billion (Hines et al. 2014).

To improve outcomes, Medicare, through its Hospital Readmissions Reduction Program (HRRP) (McIlvannan, Eapen, and Allen 2015), has targeted the reduction of readmissions that occur within the 30-days after discharge. The HRRP modifies the pre-existing inpatient payment system, penalizing readmissions. One effect of these programmatic changes has been interest in interventions surrounding transitions of care. These interventions include discharge planning services such as transfers to less-intensive healthcare institutions, as well as postdischarge outpatient interventions such as contacting the patient after discharge to check medications compliance. The availability of medical claims and electronic health records make it possible to assess the efficacy of these interventions retroactively.

## Readmission models

There exists a large body of prior work on readmission prediction based on electronic health records and medical claims. A recent review (Huang et al. 2021) surveyed properties of readmission models in the literature. By in large, they found no model type to perform consistently better than others, though many studies have found marginal improvements using either XGBoost or neural networks over logistic regression (Shameer et al. 2016; Jamei et al. 2017; Allam et al. 2019; Liu et al. 2020; Min, Yu, and Wang 2019; Futoma, Morris, and Lucas 2015). Generally, the literature has been focused on 30-day readmissions, though nuances in how readmission is defined complicate direct performance comparisons. Models in the literature based on medical claims data typically achieved AUROC of approximately 0.70 for predicting their version of all cause 30-day readmission.

The other main factor that complicates the direct comparison of modeling efforts is differences in the datasets – and hence the underlying patient populations. We are aware of two studies performed on datasets identical to ours. Lahlou et al. (2021) created an attention-based neural network for predicting admissions after discharge within 30-days and reported an AUROC value of 0.81, however, they did not distinguish between transfers, planned admissions, and acute admissions in their outcome label so they solve a different

problem that is of less practical utility. More-related to our work, MacKay et al. (2021) developed XGBoost models for predicting a set of adverse events, reporting an AUROC of 0.73 for all-cause readmission prediction.

Most studies are aware that interpretability is an important consideration in making readmission models useful. Yet, many studies that claim interpretability for their black-box solutions really offer “posthoc explainability,” a catch-all phrase for approximating narratives produced in order to promote a sense that a model is interpretable when it is not.

## Interpretability

The goal of interpretable modeling is to produce predictions that an end-user can understand (Rudin 2019, 2014) – a prerequisite for making a prediction actionable. Requirements for interpretability are application-dependent. Focusing on structured data problems in healthcare, Fig 1 is a representation of the spectrum of interpretability. A significant disconnect separates blackbox models from inherently interpretable models.

The lowest form, computational interpretability, enables one to understand how the predictors computationally interact to form a prediction. ReLU-activated neural networks (see below), matrix composition methods like principle components analysis (PCA), and large multiple regression models are all computationally interpretable, whereas Deep Learning (DL) models more-generally and ensemble trees methods like XGBoost are not. However, knowing how a prediction is computed from individual features does not automatically make the prediction comprehensible – it is generally still difficult to understand how a model behaves as there is a limit to the capacity of information that humans can process simultaneously (Miller 1956).

Beyond computational interpretability, Sudjianto and Zhang (2021) note that additivity, sparsity, linearity, smoothness, monotonicity, and visualizability are attributes shared by comprehensible models. More-generally, one might constrain the structure of the model so that it can be understood. If done using domain knowledge, such constraints can make models mechanistically meaningful. An example in computer vision is concept whitening (Chen, Bei, and Rudin 2020). Mechanistically meaningful models provide deeper insights and can easily be structured to justify causal interpretations.

**Post-hoc explainable-AI (xAI):** Posthoc xAI is a set of techniques used in an attempt to market blackbox models as interpretable, so that they falsely appear on the right side of the spectrum (Fig. 1). The most popular xAI methods (LIME (Ribeiro, Singh, and Guestrin 2016) and SHAP (Lipovetsky and Conklin 2001; Datta, Sen, and Zick 2016)), use approximations (Lundberg and Lee 2017; Aas, Jullum, and Løland 2021) to provide narratives of feature importance within a prediction. Other methods such as attention (Niu, Zhong, and Yu 2021) build an explanation mechanism as a module within a blackbox model in order to more-easily compute them (Jain and Wallace 2019; Zhou et al. 2022). Narratives, convincing as they might seem at face value, are not necessarily true. In fact, researchers

have shown (Laugel et al. 2019; Kumar et al. 2020; Slack et al. 2020; Alvarez-Melis and Jaakkola 2018; Zhou et al. 2022; Alvarez-Melis and Jaakkola 2018) that these methods provide imprecise and unreliable explanations of models. As Rudin (2019) (Rudin 2019) notes, “an explanation model that is correct 90% of the time is wrong 10% of the time.” Despite marketing claims, xAI does not carry black-box models across even a very minimal bar of requirements for interpretability. If an explanation is not true to one’s model, any sense that it is comprehensible is based on faulty information.

**Blackbox models:** Methods such as Deep Learning (DL) and ensemble boosted trees (XGBoost, LightGBM, others) can model nonlinearities. When copious training data is available, these methods yield models that are more expressive than traditional generalized linear models. Most-generally, blackbox models like DL and ensemble trees are nonlinear kernel machines (function interpolations) (Dominig 2020). What makes these methods uninterpretable is the convoluted nature of their interpolations.

Massive investment exists in these models due to their face-value performance. This investment, the challenge of creating truly interpretable models, and a myth that black-boxes perform better than interpretable models (Rudin 2019), are all factors incentivizing the marketing of posthoc-xAI as an alternative to interpretable modeling. In finance, a similarly high-stakes domain, there has been wide resistance to blackbox modeling, formalized recently in model risk management guidelines published by the Office of the Comptroller of the Currency (OCC) (The Office of the Comptroller of the Currency (OCC) 2021). Similarly, we reject the use of these models in healthcare, where the risk to patients requires truly trustworthy solutions.

**Deep learning (DL):** However, blackboxes provide clues on how to extend traditional linear models. DL is the application of artificial neural networks (ANNs) to prediction problems. ANNs consist of sequences (or more generally of graphs) of successive affine matrix arithmetic operations, sandwiched between activation functions. In general, these methods are blackboxes, with the exception of ReLU-activated neural networks (ReLU-nets for short). Examining ReLU-nets elucidates the nature of how DL captures nonlinearities. ReLU-nets use the activation function

$$\text{ReLU}(x) = 0 \text{ if } x \leq 0 \text{ or } x \text{ otherwise.} \quad (1)$$

In these models, Eq. 1 is independently applied to each matrix coordinate after each successive matrix operation. The output of the function is nonzero if and only if a linear combination of the elements computed by the prior layer are positive. Hence, ReLU defines an inequality over quantities within the model - applied to each coordinate within each layer, ReLU defines recursive sets of inequalities. These inequalities collectively segment the training data into disjoint regions. In sum, ReLU-nets are patchworks of disjoint linear models. Hence, ReLU-nets are computationally interpretable, being almost everywhere linear. The salient non-linearity of these models is locality. Observing this fact, Sudjianto et al., (Sudjianto et al. 2020) provides a tool for

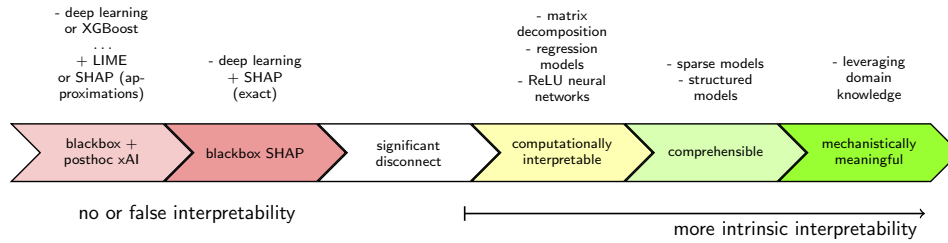


Figure 1: **Model interpretability** lies along a spectrum with a clear chasm existing between intrinsically interpretable models others. More-interpretable models are more trustworthy and insightful.

exactly interpreting trained ReLU neural networks, by unwrapping the cascades of inequalities. In this manuscript we mimic this property of ReLU-nets within a well-controlled multilevel Bayesian regression framework in order to gain expressiveness while prioritizing interpretability.

## Methods

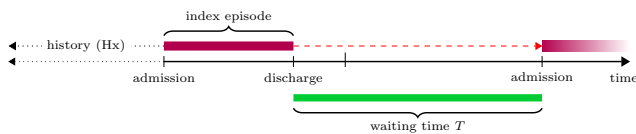


Figure 2: **The wait time  $T$**  is the time (in days) between discharge of an index episode and the next unplanned acute inpatient admission.

While readmission mitigation efforts have focused on readmissions within 30 days of discharge, we consider a broader problem of understanding the likelihood of readmission at any arbitrary day after discharge. To this end, our objective is to characterize the statistics of the inter-inpatient wait time  $T_n$  (Fig. 2). Additionally, we focus on identifying the effects of discharge placement, representing the choices symbolically as  $I_n$ , ranked in terms of health acuity:

0. discharge home
1. discharge home with home health
2. discharge to skilled nursing
3. intermediate care/critical access
4. long term care
5. other less-acute inpatient.

The issue that complicates the estimation of discharge placement effects is unobserved confounding – providers use the patient’s health status in order to decide placement. To resolve the treatment assignment bias, we model the joint outcomes

$$\begin{aligned} T_n &\sim f(T_n | \mathbf{x}_n, I_n, \boldsymbol{\alpha}_n, \boldsymbol{\beta}_n, \gamma_n) \\ I_n &\sim g(I_n | \mathbf{x}_n, \boldsymbol{\nu}_n, \boldsymbol{\xi}_n), \end{aligned} \quad (2)$$

where  $\mathbf{x}_n \in \mathbb{R}^p$  is a covariate vector and we explicitly adjust for assignment bias. Note that we distinguish between the scalar-valued  $I_n$ , which corresponds to the list of interventions above, and the vector valued  $\mathbf{I}_n$  which we will explain later in this manuscript.

For the sake of interpretability, we formulate  $f$  and  $g$  in Eq. 2 as hierarchical multilevel Bayesian generalized linear regression models. However, to increase expressivity, we allow all of the model parameters  $\boldsymbol{\alpha}_n, \boldsymbol{\beta}_n, \gamma_n, \boldsymbol{\nu}_n, \boldsymbol{\xi}_n$  to vary locally with  $\mathbf{x}_n$  in ways that comport with domain knowledge.

## Data Preprocessing

Our dataset, the CMS Limited Dataset (CMS LDS), consists of a national 5% beneficiary sample of Medicare FFS Part A and B claims from 2008 to 2012. The 2008 claims had only quarter date specificity so we used them solely to fill out the medical history for 2009 inpatient stays, by assuming that each 2008 claim fell in the middle of its given quarter. We trained the readmission models on 2009 – 2011 admissions, and evaluated the models on 2012 admissions.

After grouping claims into coherent episodes, based on date, provider, and patient overlap, we filtered for inpatient-specific episodes with certain characteristics to use as index admissions. We retained only episodes where the patient had a continuous prior year of Part A/B enrollment. We also excluded episodes from consideration as index episodes if they did not correspond to discharges to less-intensive care (excluding death and most inpatient-to-inpatient transfers). Additionally, we used the official CMS methodology for determining whether each episode is a planned admission, acute admission, or potentially planned admission (201). For each episode we then computed the waiting time to either the next unplanned acute episode or death, or until censorship due to the end of the observation window. In the end, the training dataset consisted of approximately 1.2 million inpatient episodes, of which approximately 17% were followed by an unplanned acute inpatient episode or death within 30 days. The histogram of the wait times is presented in Fig. 3.

For each episode, we collected all billing codes, creating lists of concurrent procedure and diagnostic codes. Additionally, we collected the preceding four quarters of history for each episode, aggregating billing codes on a lagged quarterly basis.

**Feature engineering:** Raw medical claims data consists of series of billing codes in several dialects (ICD9/10, HCPCS, RUG, HIPPS, etc). We down-sampled diagnostic (Dx) and procedure (Tx) codes, from their original dialects to multilevel Clinical Classification Software (CCS) codes (HCU). CCS codes are clinically curated hierarchi-

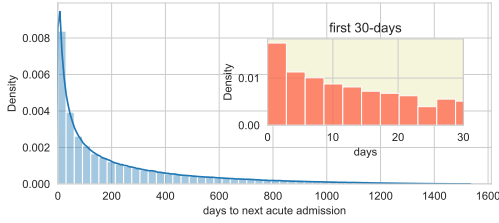


Figure 3: **Histogram of the wait time after discharge to the next acute admission or death.**

cal categories that are potentially more tractable for analysis and interpretation. Mapping to CCS drastically decreases the dimensionality of the dataset and helps to separate the health-specific information in billing codes from noisy reimbursement-specific details.

We used AHRQ Healthcare Cost and Utilization Project (HCUP) databases in order to tag codes for comorbidities, chronic conditions, surgical flags, utilization flags, and procedure flags. Included within skilled nursing facility (SNF) and home health (HH) claim codes are also activities of daily living (ADL) assessments. We converted these codes to ADL scores, where higher scores correspond to lower functional ability. We also incorporated CMS’s risk adjustment methodology, hierarchical condition categories (HCC), as model predictors.

Since the CMS LDS contains beneficiary county codes, we also incorporated the urban rural index and social economic scale as model features. Together with beneficiary race information and Medicaid state buy-in, these variables allowed for some measure of social determinants of health.

We encoded CCS and other code mappings into numerical vectors by counting the number of incidences of each permissible code. In the case of CCS, which is multilevel, we truncated codes at each of the first two levels and counted at each level. Altogether, the numerically encoded derived features constituted a vector of size  $p = 1072$ , which encompassed both concurrent episode codes and the past four quarters of history, where CCS was truncated to the first level for history.

**Feature quantization:** To improve model interpretability, we made an effort to place all model parameters (log hazard ratios) on the same scale so that the magnitudes of the parameters are directly comparable. In examining our derived data features, we came to find that they were predominantly sparse and heavy tailed. This finding, and our desire to optimize model interpretability, led us to quantize all numerical variables so that the input variables into the model are entirely binary. To this end, we first computed the percentiles for each feature across the entire dataset. Then we re-coded each quantity into a series of binary variables corresponding to inequalities, where the cutoffs were determined by examining the computed percentiles and eliminating duplicate values. Generally, we retained only the quantized features in specifying the models except when otherwise specified. The total size of the feature vector after dropping all original non-quantized numerical features and all constant fea-

tures expanded to  $p = 3143$ .

## Survival Modeling

For flexibly modeling the wait time distribution  $f$ , we use the piecewise exponential survival regression model (PEM) (Friedman 1982). As its name implies, the PEM is defined by specifying a constant hazard  $\lambda(t)$  within each time interval. The density function for the PEM is then easiest to specify by considering the cumulative hazard function  $\Lambda(t) = \int_0^t \lambda(u)du$ , and noting that  $S(t) = 1 - F(t) = e^{-\Lambda(t)}$ , where  $F(t)$  is the cumulative density function, so that

$$f(t) = \lambda(t)e^{-\Lambda(t)}. \quad (3)$$

In this manuscript we set the breakpoints at 1 week, 4 weeks, and 9 weeks.

For each episode  $n$ , we can estimate a wait time distribution by estimating the log-hazard within each time interval  $i$ ,

$$\log \lambda_{ni} = \alpha_{ni} + \beta'_{ni} \mathbf{x}_n + \gamma'_{ni} \mathbf{I}_n. \quad (4)$$

In this formulation we separate out the discharge placement effects ( $\gamma_n$ ) from other effects ( $\beta_n$ ). We do this so that we can structure the model for causally interpreting the discharge assignment effects. In addition, we utilize domain knowledge built into the ordering of the interventions, enforcing monotonicity of intervention effect by constraining the last five coefficients of  $\xi_n$  to non-positivity.

**Causal inference:** We model the discharge placement process  $g$  using an ordinal logistic regression model, where

$$\begin{aligned} I_n | \mathbf{p}_n &\sim \text{Categorical}(p_{n0}, \dots, p_{n5}) \\ p_{nk} | \mathbf{x}_n, \boldsymbol{\nu}_n, \boldsymbol{\xi}_n &= \Pr(I_n \geq k | \mathbf{x}_n, \boldsymbol{\nu}_n, \boldsymbol{\xi}_n) \\ &\quad - \Pr(I_n \geq k + 1 | \mathbf{x}_n, \boldsymbol{\nu}_n, \boldsymbol{\xi}_n) \\ \Pr(I_n \geq k | \mathbf{x}_n, \boldsymbol{\nu}_n, \boldsymbol{\xi}_n) &= \text{logit}^{-1}(\nu_{nk} + \boldsymbol{\xi}'_k \mathbf{x}_n), \end{aligned} \quad (5)$$

under the constraints  $\nu_{nk} < \nu_{n,k+1}, \forall k, n$ . The predictions given by this model then feed back into the prediction of the wait time through the covariate vector  $\mathbf{I}_n = [\Pr(I_n \geq 1 | \dots), \dots, \Pr(I_n \geq 5 | \dots), 1_{I_n \geq 1}, \dots, 1_{I_n \geq 5}]$ . Utilizing the discharge placement probabilities as model covariates adjusts for the confounding bias caused by the selection process, in a manner analogous to incorporating the local treatment probability as a covariate (Bafumi and Gelman 2007). Additionally, directly modeling the treatment effects within a multilevel model allows us to infer partially pooled locally-varying treatment effects in even regions where the data is sparse (Gelman 2006; Feller and Gelman 2015).

**Parameter decomposition:** The piecewise linear nature of ReLU-nets, and the observation that NNs produce learned data representations (Goodfellow, Bengio, and Courville 2016), suggest that an approach to mimicking their expressivity is to segment data based on learned representations and fit segmented linear models.

For segmentation, first, we project portions of the input data to lower dimensions through unsupervised methods.

In Chang et al. (2020), the authors make a connection between sparse probabilistic matrix factorization and probabilistic autoencoders. We use this approach to develop a low-dimensional representation of the portions of the input covariate vector that pertain to the lagged quarterly history. Then, we compute the statistics of the learned representation in the training data and develop for each dimension a set of cut-offs to use for bucketization. This procedure puts each inpatient episode into a specific cohort based on medical history. Specifically, we used a single cut-off (the median) for each of five dimensions (Fig. 4), creating a set of  $2^5 = 32$  groups based on history. By design, the rules governing the group assignment can be easily converted to a set of inequalities over sparse subsets of the original data features. Additionally, we interacted the history groups with other discrete attributes such as the major diagnostic category (MDC), complication or comorbidity (CC) or a major complication or comorbidity (MCC), and race, to create high dimensional discrete lattices where the cells define coarse interaction cohorts in the data.

When partitioning data by a high-order interaction, a big data problem quickly becomes many small data problems and complex models begin to suffer from overfitting – particularly when using naive divide-and-conquer approaches. To combat this issue, we developed a multiscale modeling approach, higher-order interactions are regularized by partially pooling into lower-order interactions. Specifically, given a multidimensional lattice, we assign for each parameter a value within the lattice by decomposing the value into the form

$$\theta(\kappa) = \underbrace{\theta^{(*)^5}}_{\text{zero order}} + \underbrace{\theta^{(\kappa_1, *, *, *, *)} + \theta^{(*, \kappa_2, *, *, *)} + \dots}_{\text{first order}} + \underbrace{\theta^{(\kappa_1, \kappa_2, *, *, *)} + \theta^{(\kappa_1, *, \kappa_3, *, *, *)} + \dots}_{\text{second order}} + \text{H.O.T.}, \quad (6)$$

where  $\kappa = (\kappa_1, \kappa_2, \dots, \kappa_D)$  is a  $D$  dimensional multi-index. In practice, we truncate the maximum order of terms in this decomposition due to memory constraints. More details on the exact decompositions that we used for our model parameters can be found in the Supplemental Materials.

**Statistical regularization:** By design, the parameter decomposition method inherently regularizes by partial pooling (Gelman 2006). Additionally, we used weakly informative priors on the component tensors in these decompositions in order to encourage shrinkage at higher orders. For the regression coefficients, we utilized the horseshoe prior for local-global shrinkage (Ghosh and Doshi-Velez 2017; Bhadra et al. 2019; Polson and Scott 2011; van Erp, Oberski, and Mulder 2019). Please see the Supplemental Materials for more details on the model specification.

**Implementation and computation:** We implemented our model using Tensorflow Probability (TFP) (Dillon et al. 2017), developing a set of libraries for managing the parameter decompositions that is publicly available at [github:xxxx/xxxx](https://github.com/xxxx/xxxx). The probabilistic matrix factorization method that we use for dimensionality reduction is publicly

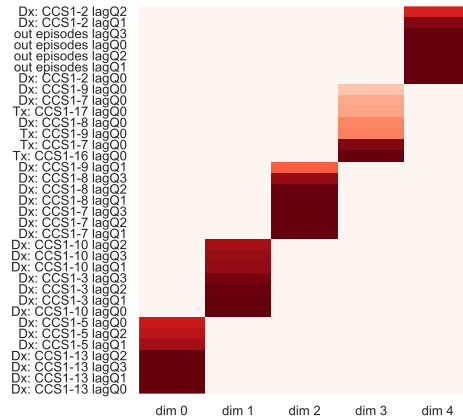


Figure 4: **History encoding weights for inpatient episodes** where the top seven variables for each dimension of a five dimensional factorization are shown. The features consist of multilevel CCS counts of diagnoses and procedures, as well as counts of the number of episodes, on a quarter-lagged basis. An episodes history representation is found by linear combination of history count features of the given weights.

available at [github:xxxx/xxxx](https://github.com/xxxx/xxxx). We used double-precision floating point for all computations performed using TFP.

We trained our model using mean-field stochastic ADVI routines present in TFP, modified for minibatch-based processing, where we used batch sizes of  $10^4$ . During training, we used a parameter sample size of 8 for approximating the variational loss function. We utilized the Adam optimizer with a starting learning rate of 0.0015, embedded within a lookahead optimizer (Zhang et al. 2019) for stability. Each epoch where the mean batch loss did not decrease, we set the learning rate to decay by 10%. Training was set to conclude if there was no improvement for 5 epochs, or if we reached 100 epochs, whichever came sooner. Generally, training concluded in approximately 80 epochs. More information on the training is present in the Supplemental Materials.

For data preprocessing, we developed a pipeline using Apache Spark 3.2.1 via the pyspark API. We used scikit-learn 1.1.1 for fitting baseline logistic regression models, and XGBoost 1.6.1 for fitting a reference blackbox model for comparison. Additionally, we implemented a horseshoe Bayesian convolution neural network with ReLU activation using TFP, where we used a single hidden layer of size one-fifth the input layer. For computing global SHAP explanations, we used regression-based KernelSHAP (Covert and Lee 2021).

All computation was performed using the Pittsburgh Supercomputing Center’s Bridges2 resources. We utilized extreme memory (EM) nodes for all data preprocessing, and Bridges2-GPU-AI for all model training.

Model	Interpretability	AUROC	AUPRC
XGBoost	None	0.758	0.497
ReLU-BNN	Computationally	0.757	0.500
LR w/o quantization	Comprehensibly	0.731	0.381
LR	Comprehensibly	0.755	0.481
<b>PEM</b>	<b>Mechanistically</b>	<b>0.757</b>	<b>0.497</b>

Table 1: **30-day unplanned readmission or death classification metrics** for evaluated models: XGBoost, Sparse logistic regression (LR), Bayesian neural network (BNN), our Piecewise exponential model (PEM). Quantization refers to the histogram-based bucketization of real-valued features. Area under the receiver operator curve (AUROC) and area under the precision-recall curve (AUPRC) computed on held-out 2012 inpatient episodes. Models trained on 2009-2011 episodes. Interpretability judged according to Fig. 1.

## Results

### Benchmarks

Table 1 shows the classification accuracy of our model in predicting readmissions or death within the first 30 days, benchmarked against predictions given by alternative models trained on the same dataset. The standard deviation in both the AUROC and AUPRC measures, as determined using bootstrap, was approximately 0.003. Quantization of the data features improved the accuracy of logistic regression to nearly match that of XGBoost on this dataset as measured by AUROC. Hence, we used quantization for features in both the Bayesian neural network (BNN) and piecewise exponential (PEM) models. The Bayesian neural network we developed utilizes sparsity-inducing horseshoe priors (Carvalho, Polson, and Scott 2010) on the weights and biases, which has been shown to improve model performance (Bhadra et al. 2019).

### Piecewise Exponential Survival Model

We discuss only select main results here. Please see the Supplemental Materials for a more-complete accounting.

The cohort-wise baseline log-hazards are presented in Fig. 5 for the 12480 episode types defined within the decomposition for the parameter vector  $\alpha_n$  in Eq. 4. Larger values of the hazard imply higher probability of event occurrence (readmission or death). As seen, there exists variability in the hazards across cohorts (rows), though the most obvious change is in time. Generally, the hazard is highest in the first week after discharge. For this reason, we will focus on understanding the model’s predictions of the first-week risk.

In the first week, the 40 most-impactful predictors of readmission are shown in Fig. 6, where the regression parameters have been decomposed in order to control for racial biases. The most-predictive single feature was length of stay. On average, lengths of stay less than a full day had a relative log hazard ratio of 0.97 (95% CI: 0.96 – 0.98). Having an acute primary diagnosis code, at least one inpatient stay in the previous quarter, and discharge against medical advice were also strong predictors associated with increased risk of readmission or death. Patients who received skilled nursing

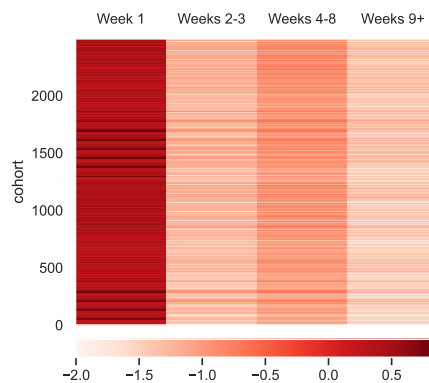


Figure 5: **Mean baseline log-hazards by week for each episode interaction cohort defined within the model.** Larger log-hazards corresponds to more readmission risk. Personalized values of  $\alpha_n$  specific to each episode are found by cohort lookup.

care in the quarter preceding an inpatient episode, who had a Resource Utilization Group (RUG) Activities of Daily Living (ADL) score of at least 6.125 tended to have a lower risk of readmission in the first week than otherwise, however, the risk increased for quarter-lagged ADL scores of at least 13.5 and concurrent ADL scores of at least 8.

**Discharge assignment effects:** In Fig. 7, we show the cohort-wise mean local average treatment effects of discharge to each of the given care settings as well as the local standard deviation in the effect. Focusing on the effect of discharging to skilled nursing care, the effects were greatest for episodes graded by DRG code as having either a complication or comorbidity (CC) or a major complication or comorbidity (MCC). In particular, CC/MCC episodes with a major diagnostic code of 2 (Diseases and Disorders of the Eye), 14 (Pregnancy, Childbirth And Puerperium), and 22 (Burns) have the greatest inferred effect for discharging to care at least as intensive as skilled nursing.

**Posthoc-xAI (SHAP):** Now that we know what the model is doing in exact terms, let us see what how posthoc-xAI thinks the model is working. In Fig. 8 we display the most important model features as determined by magnitude of global SHAP values in the prediction of readmission or death within the first 30 days. While SHAP uses approximations, it is still computationally costly to compute and the details of our SHAP computation are available in the Supplemental Materials. The four most-influential features according to the explainer are specific classes treatments and diagnoses in the recent quarterly history. Comparing these results to the parameter values of Fig. 6, it is evident that the feature sets are at complete odds. Nor do the values in Fig. 8 align with parameter values for later weeks (see Supplemental Materials). This finding is unsurprising; it has been consistently shown in any class of model where one has the ground truth interpretation (Kumar et al. 2020), so long as the features are correlated – as predictors tend to be in real-world applications. The simplest examples of this dis-

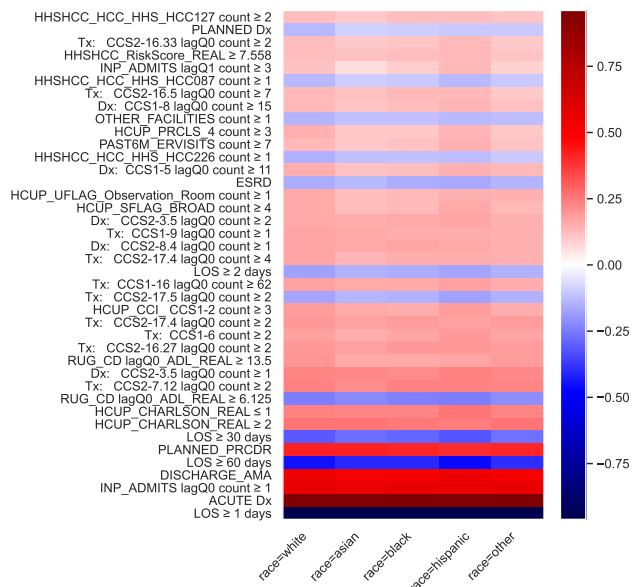


Figure 6: **The 40 predictors with the largest absolute coefficients in the first week (through day 7) after readmission.** All predictors are binary and all parameters are additive log hazard ratios. Higher (red) corresponds to larger hazards and greater readmission risk.

crepancy are within the official tutorials where SHAP is run on linear regression models (Lundberg 2022). SHAP fundamentally does not answer the question of what a given model is doing in order to reach a prediction. Furthermore, feature importance is not grounded in any relevant units and also does not speak to relevant interactions that are captured in a model. We criticize SHAP because it is one of the most popular posthoc-xAI techniques, however, similar arguments hold for other techniques (Rudin 2019; Babic et al. 2021; Zhou et al. 2022).

**Discussion**

In this manuscript, we motivated the development of a new type of expressive multilevel Bayesian regression model inspired by properties of ReLU-nets. We applied this methodology to the prediction of hospital readmissions or death after discharge, and to the causal inference of the effects of discharge assignments. We highlighted the distinction between interpretability and posthoc explainability (posthoc xAI), and demonstrated how xAI (in particular SHAP) does not aid in true model understanding. We also demonstrated how we could achieve predictive performance comparable to blackbox methods, while not sacrificing interpretability.

**Limitations:** We did not control for compliance in our effect estimates. Our modeling approach has downsides. Numerical stability generally requires the use of double precision floating point. The lattice-based parameter decomposition is memory-intensive which in some applications may severely limit expressivity.

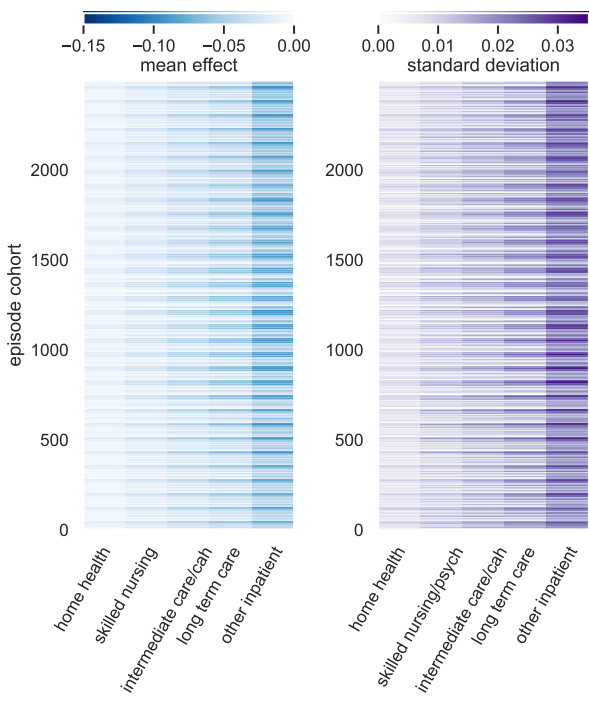


Figure 7: **First-week effects of discharge placement: Mean (left) and standard deviation (right) by cohort (row) of the five placement interventions assessed, in increasing order of implied acuity.** Effect is difference in log-hazard relative to a normal discharge (home).

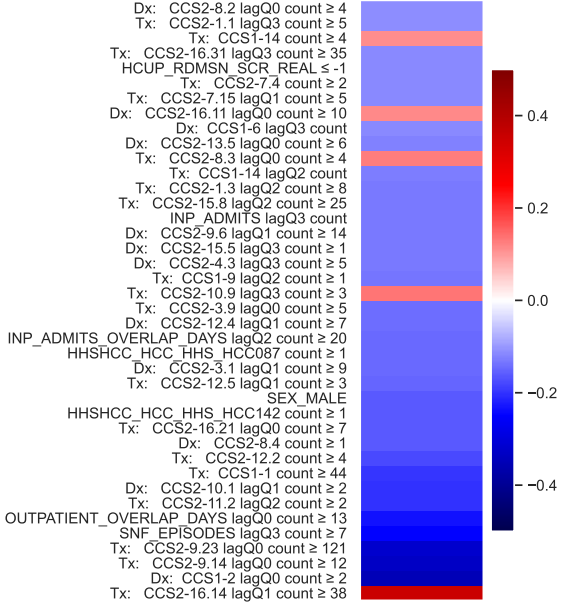


Figure 8: **Shapley values: Top 40 absolute feature weights for our survival model, where we have the ground truth explanation.**

**In defense of blackbox methods:** While posthoc-xAI does not rescue blackboxes from their uninterpretability, there are many instances where interpretability is unneeded. The quantification of a focused causal effect does not require interpretable modeling (Hill 2011), or even necessarily models at all (Ding and Miratrix 2017). Blackbox methods offer a quick way to achieve an accurate solution with minimal thoughtfulness. For these reasons, blackbox methods remain inherently useful for what they are.

### Acknowledgments

We thank the Innovation Center of the Center for Medicare and Medicaid services for providing access to the CMS Limited Dataset through DUA LDSS-2019-54177. CCC is supported by the Intramural Research Program of the NIH, NIDDK. This work used the Extreme Science and Engineering Discovery Environment (XSEDE) (Towns et al. Sept.-Oct. 2014), which is supported by National Science Foundation grant number ACI-1548562 through allocation TG-DMS190042.

### References

???? 2015 Measure Information About the 30-Day All-Cause Hospital Readmission Measure, Calculated for the Value-Based Payment Modifier Program — Guidance Portal. <https://www.hhs.gov/guidance/document/2015-measure-information-about-30-day-all-cause-hospital-readmission-measure-calculated>.

???? HCUP-US Tools & Software Page. <https://www.hcup-us.ahrq.gov/toolssoftware/ccs/ccsfactsheet.jsp>.

Aas, K.; Jullum, M.; and Løland, A. 2021. Explaining Individual Predictions When Features Are Dependent: More Accurate Approximations to Shapley Values. *Artificial Intelligence*, 298: 103502.

Allam, A.; Nagy, M.; Thoma, G.; and Krauthammer, M. 2019. Neural Networks versus Logistic Regression for 30 Days All-Cause Readmission Prediction. *Scientific Reports*, 9(1): 9277.

Alvarez-Melis, D.; and Jaakkola, T. S. 2018. On the Robustness of Interpretability Methods. *arXiv:1806.08049 [cs, stat]*.

Babic, B.; Gerke, S.; Evgeniou, T.; and Cohen, I. G. 2021. Beware Explanations from AI in Health Care. *Science*, 373(6552): 284–286.

Bafumi, J.; and Gelman, A. 2007. Fitting Multilevel Models When Predictors and Group Effects Correlate.

Bhadra, A.; Datta, J.; Li, Y.; and Polson, N. G. 2019. Horseshoe Regularization for Machine Learning in Complex and Deep Models.

Carvalho, C. M.; Polson, N. G.; and Scott, J. G. 2010. The Horseshoe Estimator for Sparse Signals. *Biometrika*, 97(2): 465–480.

Chang, J. C.; Fletcher, P.; Han, J.; Chang, T. L.; Vattikuti, S.; Desmet, B.; Zirikly, A.; and Chow, C. C. 2020. Sparse Encoding for More-Interpretable Feature-Selecting Representations in Probabilistic Matrix Factorization. In *International Conference on Learning Representations*.

Chen, Z.; Bei, Y.; and Rudin, C. 2020. Concept Whitening for Interpretable Image Recognition. *Nat Mach Intell*, 2(12): 772–782.

Covert, I.; and Lee, S.-I. 2021. Improving KernelSHAP: Practical Shapley Value Estimation via Linear Regression. *arXiv:2012.01536*.

Datta, A.; Sen, S.; and Zick, Y. 2016. Algorithmic Transparency via Quantitative Input Influence: Theory and Experiments with Learning Systems. In *2016 IEEE Symposium on Security and Privacy (SP)*, 598–617.

Dillon, J. V.; Langmore, I.; Tran, D.; Brevdo, E.; Vasudevan, S.; Moore, D.; Patton, B.; Alemi, A.; Hoffman, M.; and Saurous, R. A. 2017. TensorFlow Distributions. *arXiv:1711.10604 [cs, stat]*.

Ding, P.; and Miratrix, L. W. 2017. Model-Free Causal Inference of Binary Experimental Data. *arXiv:1705.08526*.

Domingos, P. 2020. Every Model Learned by Gradient Descent Is Approximately a Kernel Machine. *arXiv:2012.00152 [cs, stat]*.

Feller, A.; and Gelman, A. 2015. Hierarchical Models for Causal Effects. In *Emerging Trends in the Social and Behavioral Sciences*, 1–16. John Wiley & Sons, Ltd. ISBN 978-1-118-90077-2.

Friedman, M. 1982. Piecewise Exponential Models for Survival Data with Covariates. *Ann. Statist.*, 10(1): 101–113.

Futoma, J.; Morris, J.; and Lucas, J. 2015. A Comparison of Models for Predicting Early Hospital Readmissions. *Journal of Biomedical Informatics*, 56: 229–238.

Gelman, A. 2006. Multilevel (Hierarchical) Modeling: What It Can and Cannot Do. *Technometrics*, 48(3): 432–435.

Ghosh, S.; and Doshi-Velez, F. 2017. Model Selection in Bayesian Neural Networks via Horseshoe Priors. *arXiv:1705.10388 [stat]*.

Goodfellow, I.; Bengio, Y.; and Courville, A. 2016. *Deep Learning*. MIT Press. ISBN 978-0-262-33737-3.

Hill, J. L. 2011. Bayesian Nonparametric Modeling for Causal Inference. *Journal of Computational and Graphical Statistics*, 20(1): 217–240.

Hines, A.; Barrett, M.; Jiang, J.; and Steiner, C. 2014. Conditions With the Largest Number of Adult Hospital Readmissions by Payer, 2011. Technical Report #172.

Huang, Y.; Talwar, A.; Chatterjee, S.; and Aparasu, R. R. 2021. Application of Machine Learning in Predicting Hospital Readmissions: A Scoping Review of the Literature. *BMC Medical Research Methodology*, 21(1): 96.

Jain, S.; and Wallace, B. C. 2019. Attention Is Not Explanation. *arXiv:1902.10186*.

Jamei, M.; Nisnevich, A.; Wetchler, E.; Sudat, S.; and Liu, E. 2017. Predicting All-Cause Risk of 30-Day Hospital Readmission Using Artificial Neural Networks. *PLoS One*, 12(7).

Kumar, I. E.; Venkatasubramanian, S.; Scheidegger, C.; and Friedler, S. 2020. Problems with Shapley-value-based Explanations as Feature Importance Measures. *arXiv:2002.11097 [cs, stat]*.

- Lahlou, C.; Crayton, A.; Trier, C.; and Willett, E. 2021. Explainable Health Risk Predictor with Transformer-based Medicare Claim Encoder. *arXiv:2105.09428*.
- Laugel, T.; Lesot, M.-J.; Marsala, C.; Renard, X.; and Detryniecki, M. 2019. The Dangers of Post-hoc Interpretability: Unjustified Counterfactual Explanations. *arXiv:1907.09294 [cs, stat]*.
- Lipovetsky, S.; and Conklin, M. 2001. Analysis of Regression in Game Theory Approach. *Applied Stochastic Models in Business and Industry*, 17(4): 319–330.
- Liu, W.; Stansbury, C.; Singh, K.; Ryan, A. M.; Sukul, D.; Mahmoudi, E.; Waljee, A.; Zhu, J.; and Nallamothu, B. K. 2020. Predicting 30-Day Hospital Readmissions Using Artificial Neural Networks with Medical Code Embedding. *PLoS One*, 15(4).
- Lundberg, S. 2022. Slundberg/Shap.
- Lundberg, S. M.; and Lee, S.-I. 2017. A Unified Approach to Interpreting Model Predictions. In *Advances in Neural Information Processing Systems*, volume 30. Curran Associates, Inc.
- MacKay, E. J.; Stubna, M. D.; Chivers, C.; Draugelis, M. E.; Hanson, W. J.; Desai, N. D.; and Groeneveld, P. W. 2021. Application of Machine Learning Approaches to Administrative Claims Data to Predict Clinical Outcomes in Medical and Surgical Patient Populations. *PLOS ONE*, 16(6): e0252585.
- McIlvennan, C. K.; Eapen, Z. J.; and Allen, L. A. 2015. Hospital Readmissions Reduction Program. *Circulation*, 131(20): 1796–1803.
- Miller, G. A. 1956. The Magical Number Seven plus or Minus Two: Some Limits on Our Capacity for Processing Information. *Psychological review*.
- Min, X.; Yu, B.; and Wang, F. 2019. Predictive Modeling of the Hospital Readmission Risk from Patients’ Claims Data Using Machine Learning: A Case Study on COPD. *Scientific Reports*, 9(1): 2362.
- Niu, Z.; Zhong, G.; and Yu, H. 2021. A Review on the Attention Mechanism of Deep Learning. *Neurocomputing*, 452: 48–62.
- Polson, N. G.; and Scott, J. G. 2011. *Shrink Globally, Act Locally: Sparse Bayesian Regularization and Prediction* \*. Oxford University Press. ISBN 978-0-19-173192-1.
- Ribeiro, M. T.; Singh, S.; and Guestrin, C. 2016. “Why Should I Trust You?”: Explaining the Predictions of Any Classifier. *arXiv:1602.04938 [cs, stat]*.
- Rudin, C. 2014. Algorithms for Interpretable Machine Learning. In *Proceedings of the 20th ACM SIGKDD International Conference on Knowledge Discovery and Data Mining*, KDD ’14, 1519. New York, NY, USA: Association for Computing Machinery. ISBN 978-1-4503-2956-9.
- Rudin, C. 2019. Stop Explaining Black Box Machine Learning Models for High Stakes Decisions and Use Interpretable Models Instead. *Nature Machine Intelligence*, 1(5): 206–215.
- Shameer, K.; Johnson, K. W.; Yahi, A.; Miotto, R.; Li, L.; Ricks, D.; Jebakaran, J.; Kovatch, P.; Sengupta, P. P.; Gelijs, S.; Moskovitz, A.; Darrow, B.; David, D. L.; Kasarskis, A.; Tatonetti, N. P.; Pinney, S.; and Dudley, J. T. 2016. Predictive Modeling of Hospital Readmission Rates Using Electronic Medical Record-Wide Machine Learning: A Case-Study Using Mount Sinai Heart Failure Cohort. In *Bio-computing 2017*, 276–287. WORLD SCIENTIFIC. ISBN 978-981-320-780-6.
- Slack, D.; Hilgard, S.; Jia, E.; Singh, S.; and Lakkaraju, H. 2020. Fooling LIME and SHAP: Adversarial Attacks on Post Hoc Explanation Methods. *arXiv:1911.02508 [cs, stat]*.
- Sudjianto, A.; Knauth, W.; Singh, R.; Yang, Z.; and Zhang, A. 2020. Unwrapping The Black Box of Deep ReLU Networks: Interpretability, Diagnostics, and Simplification. *arXiv:2011.04041 [cs, stat]*.
- Sudjianto, A.; and Zhang, A. 2021. Designing Inherently Interpretable Machine Learning Models. *arXiv:2111.01743*.
- The Office of the Comptroller of the Currency (OCC). 2021. Comptroller’s Handbook: Model Risk Management. In *Comptroller’s Handbook*, Safety and Soundness.
- Towns, J.; Cockerill, T.; Dahan, M.; Foster, I.; Gaither, K.; Grimshaw, A.; Hazlewood, V.; Lathrop, S.; Lifka, D.; Peterson, G. D.; Roskies, R.; Scott, J. R.; and Wilkins-Diehr, N. Sept.-Oct. 2014. XSEDE: Accelerating Scientific Discovery. *Computing in Science & Engineering*, 16(5): 62–74.
- van Erp, S.; Oberski, D. L.; and Mulder, J. 2019. Shrinkage Priors for Bayesian Penalized Regression. *Journal of Mathematical Psychology*, 89: 31–50.
- Zhang, M. R.; Lucas, J.; Hinton, G.; and Ba, J. 2019. Lookahead Optimizer: k Steps Forward, 1 Step Back.
- Zhou, Y.; Booth, S.; Ribeiro, M. T.; and Shah, J. 2022. Do Feature Attribution Methods Correctly Attribute Features? *Proceedings of the AAAI Conference on Artificial Intelligence*, 36(9): 9623–9633.

## Supplementary Methods

### Medicare data preprocessing

Here we describe some details on the choices we made in preprocessing that will help make our work reproducible. Kyle Barron’s Medicare Documentation repository of Medicare data documentation is an excellent resource for acquainting oneself with this standardized dataset. Our first steps in processing the CMS LDS were to merge the files, originally organized by year, into long tables for each claim type. In the process, we renamed pre-2011 columns in the dataset to match 2011+ plus columns where-ever they differed. We will refer to the dataset using 2011 and beyond column names.

**Episode Grouping** The CMS LDS consists of records organized into claims. Multiple claims can constitute a single period or episode of service. We determined episodes of the following types:

1. inpatient (inp)
2. skilled nursing facility (snf)
3. hospice (hosp)
4. outpatient (out, car)

For determining episodes, we grouped claims of each of the given types by person, and sorted by either the admission date (for inp, snf, hosp), or the claim through-date for (out, car).

Then for inp, snf, hosp, we merged successive claims into running episodes if they overlapped temporally, if the provider was the same and the intermediate discharge code indicates that the individual was not otherwise discharged home in between (we allow for distinct episodes with zero days of wait if a patient is discharged home and returns on the same day).

For out and car, we did the same merging with all claim types together, relaxing the need for the provider to match in an episode. Then we filtered for out/car episodes that did not overlap with inp, snf, hosp episodes – we determined these to be true outpatient episodes.

Then, for out and inp episodes, we determined if they corresponded to emergency department visits by looking for corresponding revenue center codes.

### Model Specification

Parameter	Decomposition	Max order
$\alpha$	MDC $\times$ Hx $\times$ CC/MCC	2
$\beta$	race	1
$\gamma$	MDC $\times$ Hx $\times$ CC/MCC	2
$\nu$	MDC $\times$ Hx $\times$ CC/MCC	2

Table 2: **Specific decompositions used per parameter to define cohorts**, where major diagnostic category (MDC) is of size 26, history (Hx) is of size  $2^5$ , corresponding to low/high in each of the five dimensions, CC/MCC is of size 3, and race is of size 5.

The specific decompositions that we used for each of the model terms are displayed in Fig. 2. For the missing parameter  $\xi$ , the results in this manuscript are all determined using  $\xi = 0$ .

The python package `bayesianquilts`, with demonstration available at `github:xxxxx/bayesianquilts` contains utilities for managing decompositions such as these.

We used a regularized horseshoe prior in order to encourage  $\beta$  to be sparse. Specifically, we applied an independent horseshoe prior to this parameter within every model cohort.

The individual components of each of the parameter decompositions were all modeled using Gaussian weakly-informative priors (with a default scale of 5 for the zero-order terms in the expansion). We helped encourage shrinkage by having the scale of these priors decay for higher order terms in the decomposition. For the results in the paper, we used a decay factor of 0.1 per each order.

**Training** We utilize TFP’s ADVI routines, which utilize stochastic sampling in computation of the ELBO. For this reason, it is not uncommon for specific parameter combinations to be in highly improbable locations – which can trigger underflows. To avoid instabilities, re adjust the likelihood on a per-observation level, first computing the minimum finite value of the log likelihood and then setting any divergent values to the minimum finite value minus a fixed offset of 100. We use the soft-plus function as a default bijector for any parameters that are supposed to be non-negative.

**SHAP** KernelSHAP, the general all-purpose model-agnostic implementation of SHAP, is very resource intensive, so we had to tune it in order to run it. First, we used the regression-based version of KernelSHAP, found in the python package `shapreg`, which is not as resource intensive.

Second, although we had a very powerful computational resource at our disposal (Pittsburgh Supercomputer Center Bridges 2-AI with 512GB RAM), we had to restrict the input data size to 5k random training examples. Otherwise, we found that the system would run out of memory, causing the application to segmentation fault.

Finally, in order to get around an error involving a singular matrix, we regularized the linear algebra problem embedded within the algorithm, adding a fixed small constant of  $10^{-8}$  to the diagonal of the linear transformation matrix (see `github:xxxxx/shapley-regression`) for the exact modification made.

We were able to run `shapref` with `n_samples=2400` and `batch_size=24` on our resource in approximately 5 hours. Due to the memory requirement issues with our large dataset, we are not able to scale this result to more data. SHAP is known to be computationally expensive, particularly for large datasets and a large number of features (see `github issues 1053 1495`), and its very computation is inherently based on approximations. We believe that our computation of SHAP for our model is a reasonable representation of how well-approximated it is in practice, on a real problem and on a real dataset with a large number of predictors.

Our main point in the main text is a reiteration of the well-known fact that SHAP feature importance is not guaranteed to match what a model is doing in practice when the features in the training data are correlated – as would be true in most real-world problems. Examining Fig. 8 in the context of Fig. S6, one sees that the most-important SHAP features are not themselves very important in the model.

## Supplementary Results

Here are results omitted from the main text for space constraints.

### History representation

We utilized sparse probabilistic matrix factorization in order to obtain a low-dimension representation of personal medical history for the year prior to each episode. The encodings given by the model (Fig. S1 is an expanded version of Fig. 4 from the main text) specify linear combinations of the original data features that define a representation of an episode’s history. The representations then can be constituted into a predictive distribution for the original features by transformation against a decoding matrix (Fig. S2). Note that this method finds a subset of the input features that can be used to predict the value of all features.

**Random slopes** Although we do not use this terminology in the main text, in the language of hierarchical mixed effects models the parameters  $\beta$ ,  $\xi$  in the model are random slopes. In the main text we presented the week 1 slopes in Fig. 6. In Fig. S3, we present the components of  $\beta$  of the largest magnitudes, across all time intervals. As we noted in the main text, length of stay being at least 1 day, or conversely, being less than a full day, was the most impact predictor of early readmission. However, the effect disappears after one week. Long length of stay (greater than 30 days) appeared to follow the same trend, with those having a length of stay of at least a month having a lower readmission risk in the first week after discharge, but not reduced risk after the first week. Generally, the magnitude of the slopes tended to increase over time, with a few exceptions.

**Random intercepts** The parameter  $\alpha$  from Eq. 4 is specific to each cohort in the model – it is a random intercept in hierarchical mixed effects modeling terminology. We presented the posterior mean for this parameter in Fig. 5, interpreting this quantity as a cohort-specific baseline survival.

**Causal inference** In our model we adjust for treatment selection bias by incorporating estimates of the treatment probabilities as covariates. The ordinal logistic regression intercepts are provided in Fig. S4.

The first five components in the parameter  $\gamma$  adjust for the selection bias present in claims. We present our cohort-specific estimates of  $\gamma$  in Fig. S5. We present the full time-course of discharge placement effects in Fig. S6. Largely, the discharge placement effects appear to strengthen from week 1 to weeks 2/3 before weakening from week four onwards. The discharge placement bias effects have more cohort-level variability after the first week. In Fig. S7, we zoom in on the effects for the cohorts that benefit the most from the

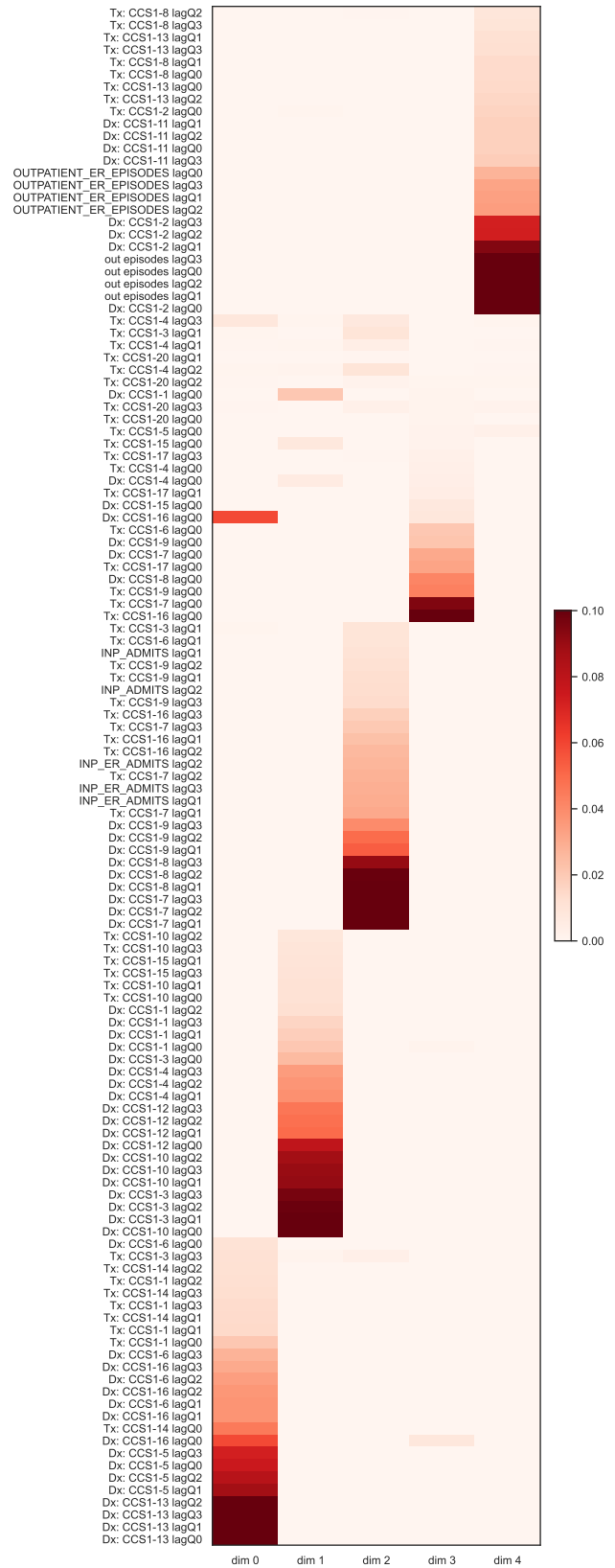


Figure S1: **Extended version of Fig. 4** with up to 25 features per dimension

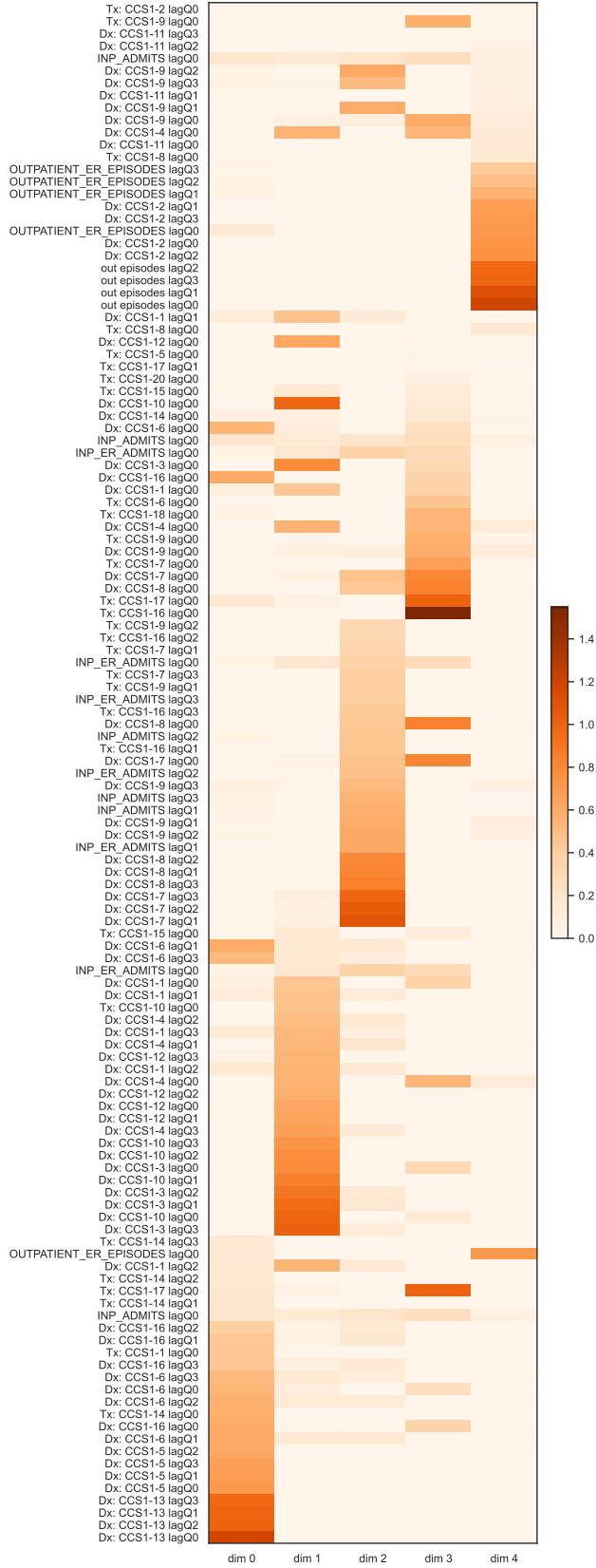


Figure S2: Decoding matrix corresponding to the encoding model of Fig. S1 showing up 25 features per dimension

discharge placement interventions. A key advantage of this form of modeling against even the computationally interpretable ReLU-nets is the ability to perform mesoscopic cohort-level inference and interpretation. Cohort-level information facilitates making a model actionable since actions can be applied to subgroups all at once.

### Priors for the decomposition

Let

$$\theta^{(\kappa)} = \sum_{o=0}^O \theta_o^{(\kappa)}, \quad (7)$$

where  $\mathbb{E}(\theta_0^{(\kappa)}) = \mu_o^{(\kappa)}, \forall o \leq O$ . Suppose that for two multi-indices  $\kappa_1, \kappa_2$ , that

- $\theta_o^{(\kappa_1)} = \theta_o^{(\kappa_2)}, \forall o \leq U < O$
- $\text{Cov}(\theta_j^{(\kappa_1)}, \theta_k^{(\kappa_2)}) = 0$  if  $j \neq k$
- $\text{Var}(\theta_o^{(\kappa)}) = \sigma_o^2$

Then,

$$\begin{aligned} \text{Cov}(\theta^{(\kappa_1)}, \theta^{(\kappa_2)}) &= \sum_j \sum_k \text{Cov}(\theta_j^{(\kappa_1)}, \theta_k^{(\kappa_2)}) \\ &= \left( \sum_{j=0}^U \sum_{k=0}^U + \sum_{j=U+1}^O \sum_{k=0}^U + \sum_{j=0}^U \sum_{k=U+1}^O \right) \text{Cov}(\theta_j^{(\kappa_1)}, \theta_k^{(\kappa_2)}) \\ &= \sum_{o=0}^U \sigma_o^2 + \sum_{o=U+1}^O \text{Cov}(\theta_o^{(\kappa_1)}, \theta_o^{(\kappa_2)}). \end{aligned} \quad (8)$$

So,

$$\begin{aligned} \rho(\theta^{(\kappa_1)}, \theta^{(\kappa_2)}) &= \frac{\sum_{o=0}^U \sigma_o^2 + \sum_{o=U+1}^O \text{Cov}(\theta_o^{(\kappa_1)}, \theta_o^{(\kappa_2)})}{\sum_{o=0}^O \sigma_o^2} \\ &= \frac{\sum_{o=0}^U \sigma_o^2 + \sum_{o=U+1}^O \rho_o \sigma_o^2}{\sum_{o=0}^O \sigma_o^2} \end{aligned} \quad (9)$$

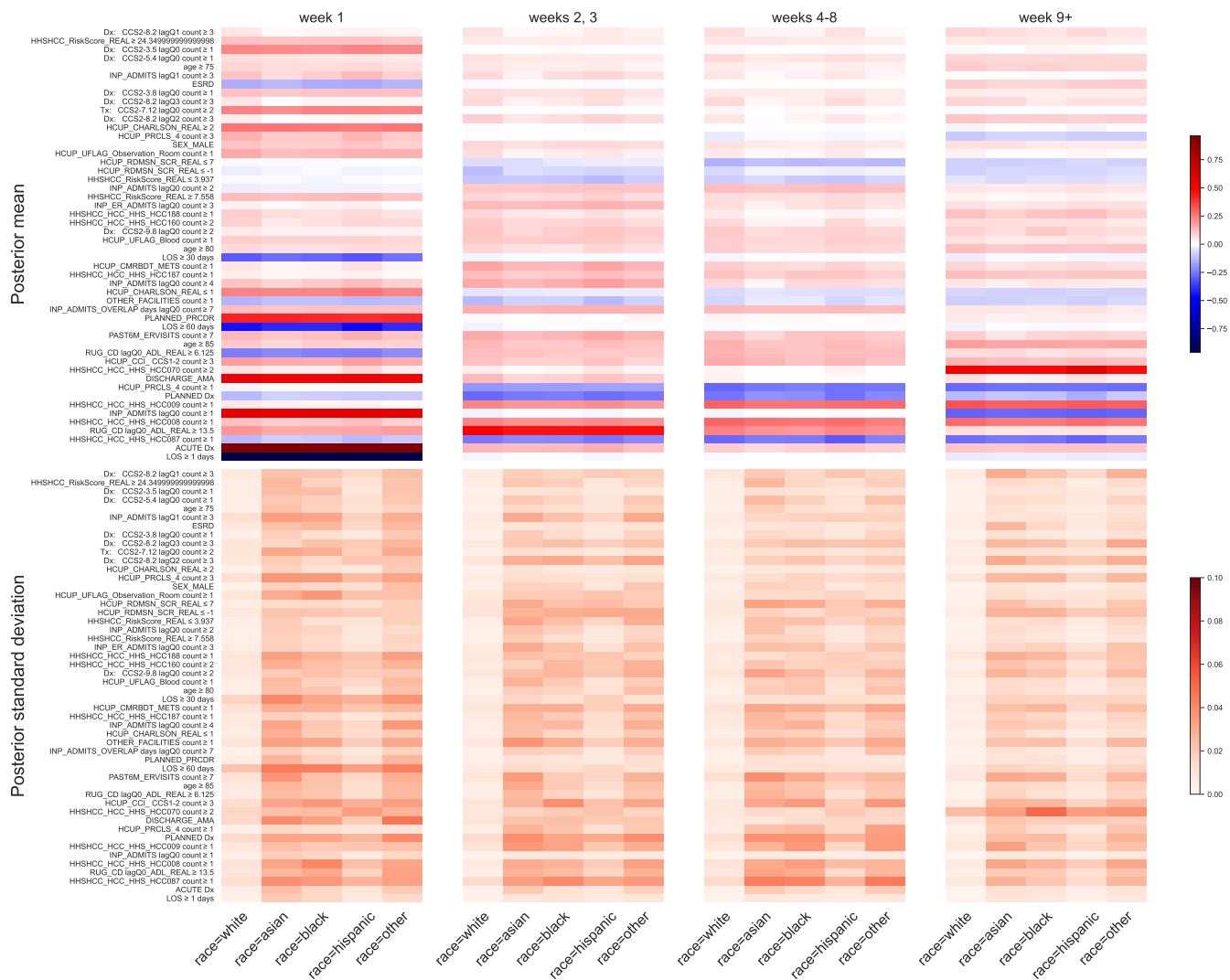


Figure S3: **The 50 most influential regressors  $\beta$  (posterior mean, standard deviation)** tracked through all time intervals. A more-comprehensive version of this figure can be found in our other supplemental file.

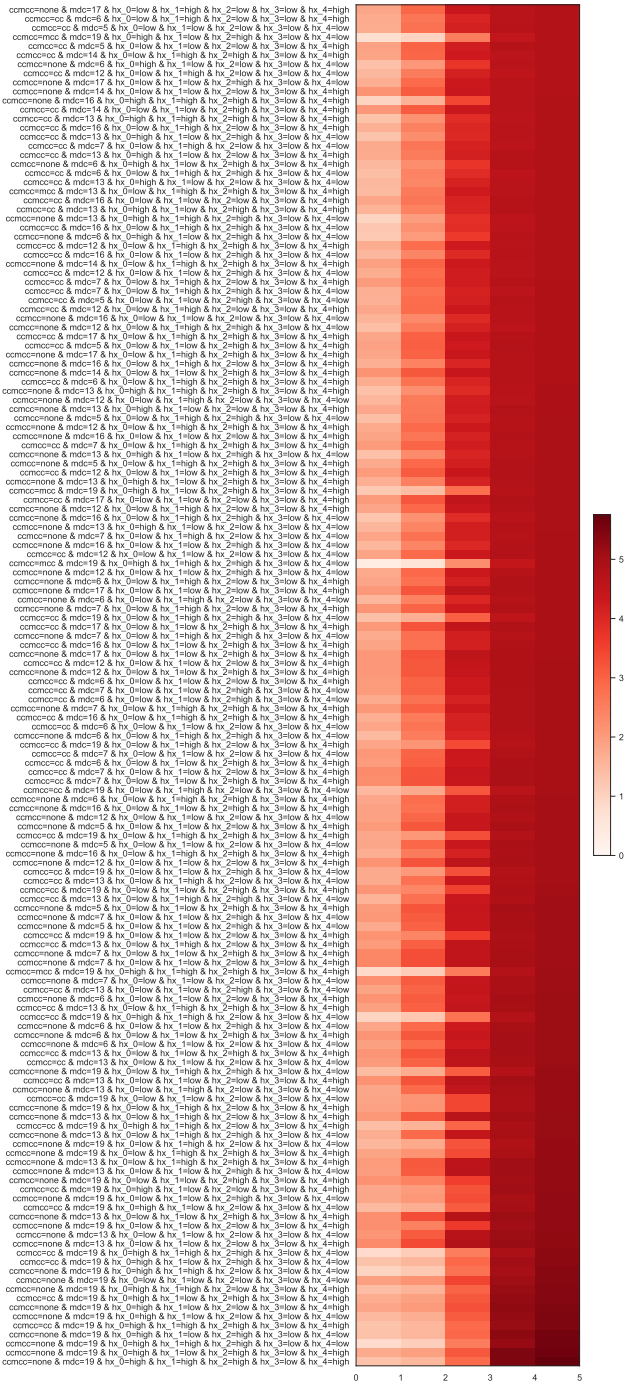


Figure S4: Cohort-wise ordinal intercept terms  $\nu$  for the prediction of the distribution of discharge assignments.

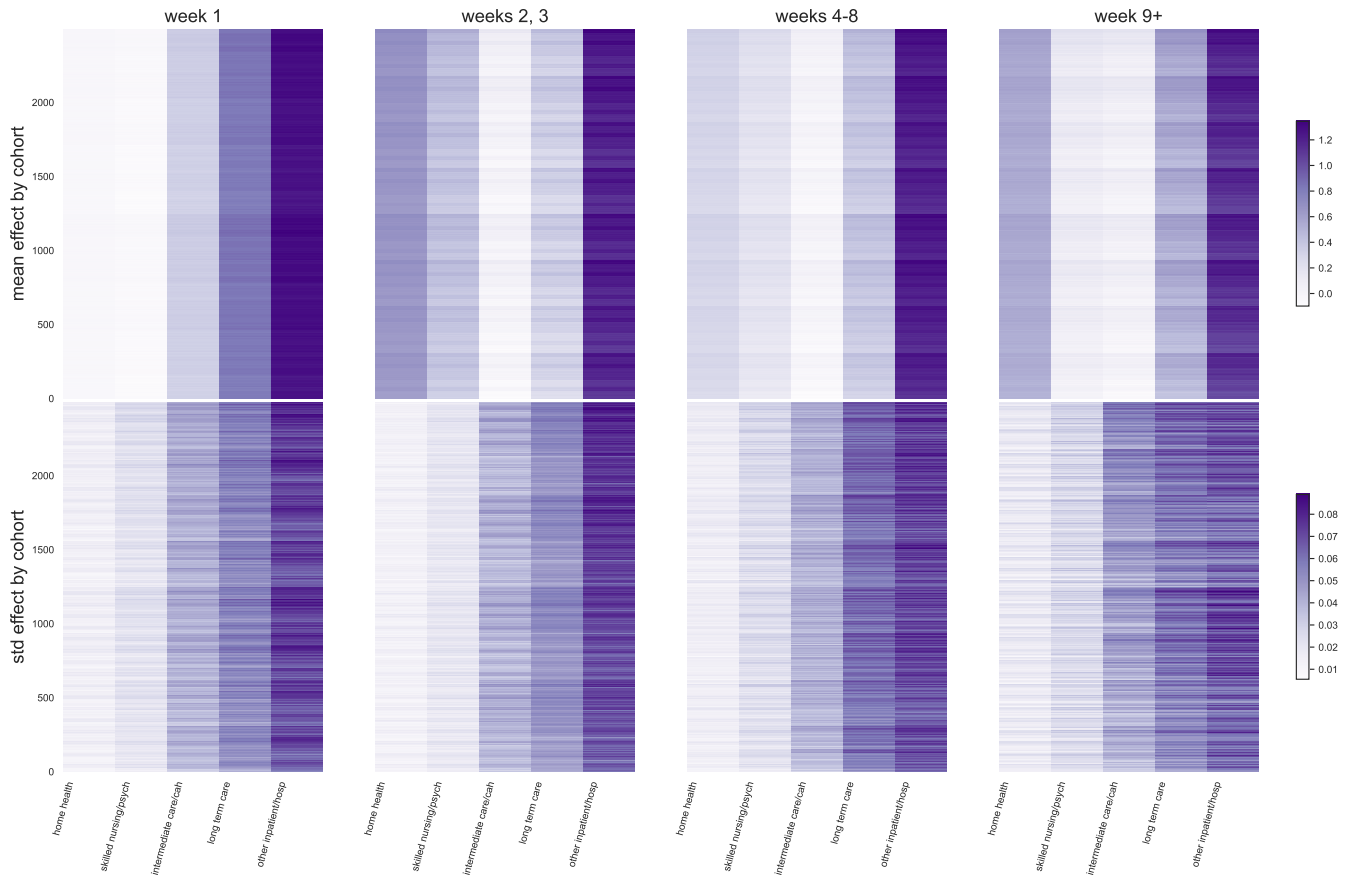


Figure S5: **Discharge assignment adjustment terms corresponding to first five terms of  $\gamma$  (posterior mean, standard deviation) in terms of log hazard ratio under the log-additive effects model of Eq. 4**

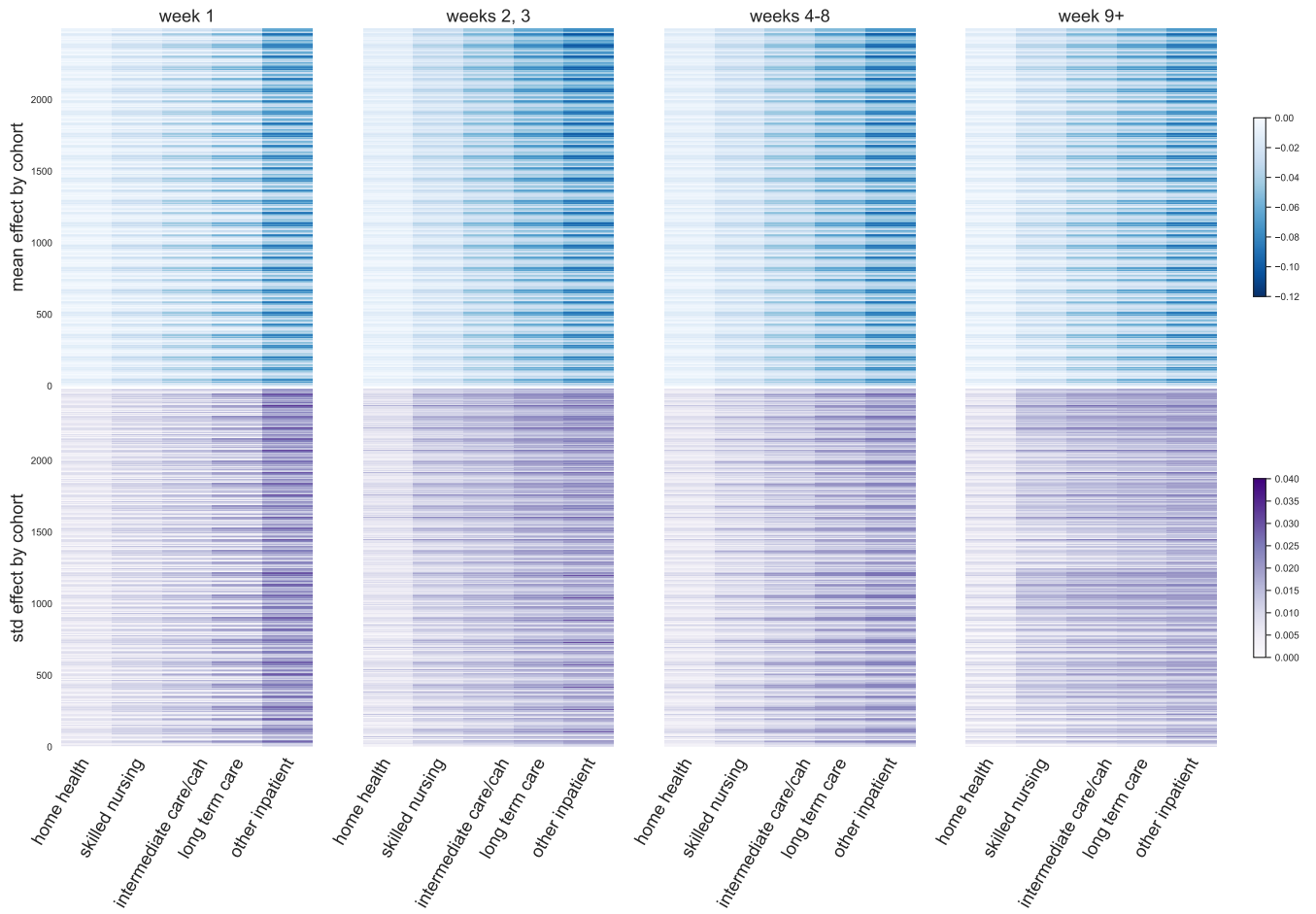


Figure S6: **Discharge placement effects  $\gamma$  (posterior mean, standard deviation)** in terms of log hazard ratio under the log-additive effects model of Eq. 4

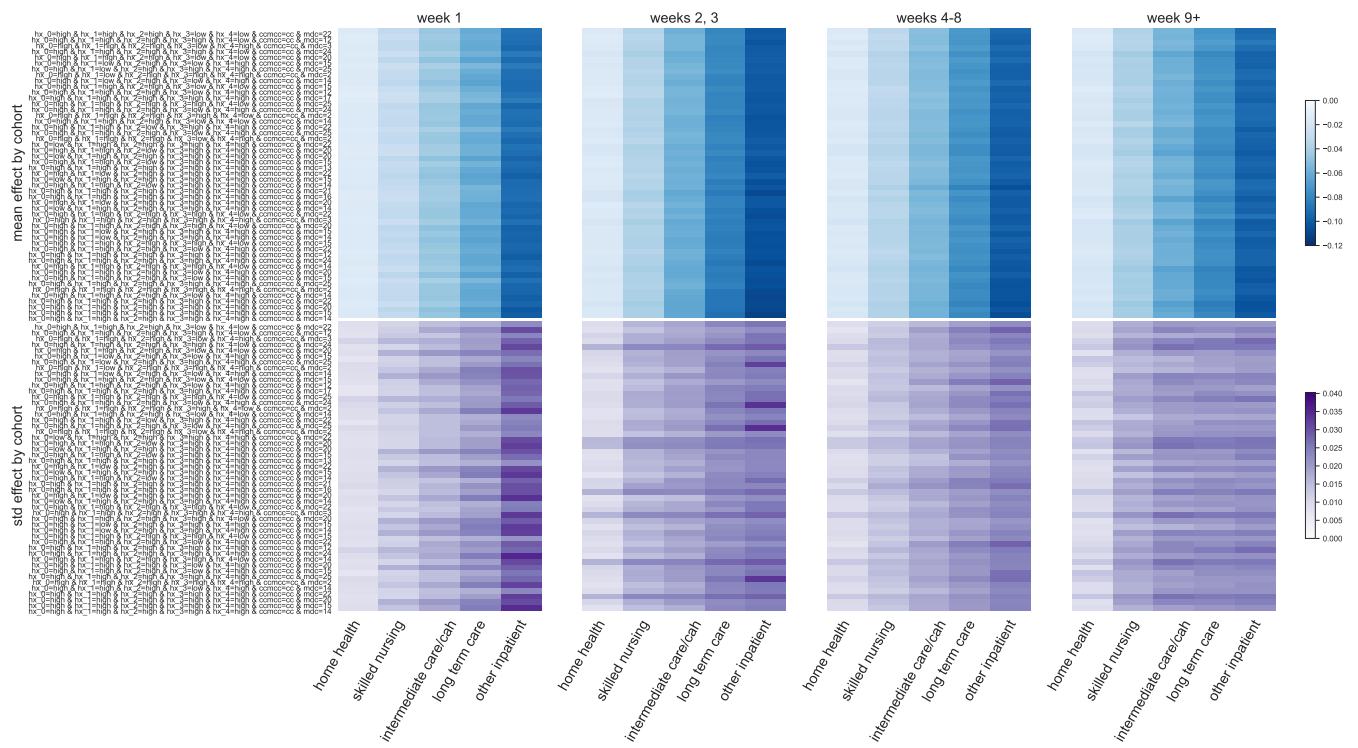


Figure S7: **Discharge placement effects for select cohorts** with the largest mean discharge placement effects.